

# Revisiting the temperature and neutron density conditions for $r$ -process nucleosynthesis with augmented nuclear mass models

X. D. Xu<sup>1</sup>, B. Sun<sup>1,2,\*</sup>, Z. M. Niu<sup>3</sup>, Z. Li<sup>1</sup>, Y.-Z. Qian<sup>4,1,†</sup> and J. Meng<sup>1,5,6‡</sup>

<sup>1</sup>*School of Physics and Nuclear Energy Engineering,  
Beihang University, Beijing 100191, China*

<sup>2</sup>*Justus-Liebig-Universität Giessen, Heinrich-Buff-Ring 14, Giessen 35392, Germany*

<sup>3</sup>*Department of Physics, Anhui University, Hefei 230601, China*

<sup>4</sup>*School of Physics and Astronomy, University of Minnesota,  
Minneapolis, Minnesota 55455, USA*

<sup>5</sup>*State Key Laboratory of Nuclear Physics and Technology,  
School of Physics, Peking University, Beijing 100871, China and*

<sup>6</sup>*Department of Physics, University of Stellenbosch, Stellenbosch, South Africa*

(Dated: August 14, 2012)

## Abstract

We explore the effects of nuclear masses on the temperature and neutron density conditions required for  $r$ -process nucleosynthesis using four nuclear mass models augmented by the latest atomic mass evaluation. For each model we derive the conditions for producing the observed abundance peaks at mass numbers  $A \sim 80$ , 130, and 195 under the waiting-point approximation and further determine the sets of conditions that can best reproduce the  $r$ -process abundance patterns ( $r$ -patterns) inferred for the solar system and observed in metal-poor stars of the Milky Way halo. We find that (1) the conditions for producing abundance peaks at  $A \sim 80$  and 195 tend to be very different, which suggests that these two peaks are not produced simultaneously; (2) the typical conditions required by the critical waiting-point (CWP) nuclei with the  $N = 126$  closed neutron shell overlap significantly with those required by the  $N = 82$  CWP nuclei, which enables coproduction of abundance peaks at  $A \sim 130$  and 195 in accordance with observations of many metal-poor stars; and (3) the typical conditions required by the  $N = 82$  CWP nuclei can reproduce the  $r$ -pattern observed in the metal-poor star HD 122563, which differs greatly from the solar  $r$ -pattern. We also examine how nuclear mass uncertainties affect the conditions required for the  $r$ -process and identify some key nuclei including  $^{76}\text{Ni}$  to  $^{78}\text{Ni}$ ,  $^{82}\text{Zn}$ ,  $^{131}\text{Cd}$ , and  $^{132}\text{Cd}$  for precise mass measurements at rare-isotope beam facilities.

PACS numbers: 26.30.Hj, 21.10.Dr, 97.10.Tk

---

\*e-mail: bhsun@buaa.edu.cn

†e-mail: qian@physics.umn.edu

‡e-mail: mengj@pku.edu.cn

## I. INTRODUCTION

Nucleosynthesis via rapid neutron capture, the  $r$ -process, is a major mechanism for producing the elements heavier than Fe [1, 2]. Understanding this process requires knowledge of properties such as masses,  $\beta$ -decay lifetimes, and neutron-capture cross sections for a large number of extremely neutron-rich nuclei far from stability (e.g., [3–5]). Most of this nuclear input is beyond the reach of experiments in the foreseeable future and therefore, must be calculated with guidance from existing data and from measurements to be made at rare-isotope beam facilities such as FRIB, RIKEN, and FAIR. In this paper we explore the importance of nuclear masses in estimating the temperature and neutron density conditions required for a specific  $r$ -process scenario, where neutron-capture reactions are in equilibrium with the reverse photo-disintegration reactions, i.e., there is  $(n, \gamma) \rightleftharpoons (\gamma, n)$  equilibrium (e.g., [3–5]). Using four nuclear mass models, we show that the required conditions can be determined mostly from the neutron-separation energies for a small number of critical nuclei with  $N = 50, 82$ , and  $126$  closed neutron shells. For each model, we further determine the best-fit sets of conditions to reproduce the  $r$ -process abundance pattern ( $r$ -pattern) inferred for the solar system and observed in metal-poor stars of the Milky Way halo. This allows us to draw several interesting conclusions regarding the production of different parts of the overall  $r$ -pattern in an  $(n, \gamma) \rightleftharpoons (\gamma, n)$ -equilibrium scenario. We also illustrate the effects of nuclear mass uncertainties on the required  $r$ -process conditions and identify the key nuclei that have the largest impact and therefore, are important candidates for precise mass measurements at rare-isotope beam facilities.

We first give a brief overview of the  $r$ -process. Detailed reviews can be found in Ref. [3–5]. Historically, the abundance distribution of nuclei in the solar system played a crucial role in studies on the origin of the elements [1, 2]. One of the prominent features of this distribution is the presence of three sets of double peaks in the region beyond the Fe group nuclei. This was recognized as signatures of two distinct processes of neutron capture: a slow ( $s$ ) one encountering the  $N = 50, 82$ , and  $126$  closed neutron shells in the stable region and a rapid ( $r$ ) one encountering the same in the extremely neutron-rich region of the nuclear chart [1, 2]. Specifically, the peaks at mass numbers  $A \sim 80, 130$ , and  $195$  were produced by the  $r$ -process and represent the crucial features of the solar  $r$ -pattern, which is derived by subtracting the  $s$ -process contributions from the net solar abundances (e.g., [6]).

In order to fully understand the  $r$ -process, we need conditions such as temperature and neutron density in the associated astrophysical environments in addition to the properties of a large number of extremely neutron-rich nuclei. Neither the astrophysical nor the nuclear input is firmly established, although much progress has been made over the past two decades [3–5]. Proposed astrophysical sites for the  $r$ -process include neutrino-driven winds from proto-neutron stars formed in core-collapse supernovae (CCSNe) [7–9], shocked surface layers of O-Ne-Mg cores associated with low-mass CCSNe [10], winds from accretion disks of black holes formed in high-mass CCSNe [11–14], He shells of metal-poor CCSNe [15, 16], and ejecta from neutron star mergers [17–20]. There are large uncertainties in the conditions associated with all CCSNe environments due to the substantial uncertainties in modeling such environments (e.g., [21]), especially when neutrino transport in hot and dense nuclear matter is considered (e.g., [22, 23]). While recent studies lend much support to neutron star mergers being an  $r$ -process site [17–20], it remains to be seen whether such models are consistent with the history of  $r$ -process enrichments in the Milky Way and in its satellite dwarf galaxies (e.g., [24–26]). Further, how sensitive these models are to the uncertainties in the current understanding of the nuclear equation of state (e.g., [27]) and to the numerical treatment of the merger dynamics remains to be studied in detail.

The conditions in the astrophysical environments relevant for the  $r$ -process ultimately boil down to the seed nuclei for neutron capture at the beginning of the process and the temperature  $T(t)$  and the neutron (number) density  $n_n(t)$  as functions of time  $t$  during the process (e.g., [28]). In cases where neutrino interactions are important, the time evolution of neutrino fluxes and energy spectra is also required (e.g., [15, 16]). In the rest of the paper we will ignore neutrinos and focus on a broad class of astrophysical environments where matter undergoes  $r$ -processing at  $T \gtrsim 10^9$  K and  $n_n \gtrsim 10^{20}$  cm $^{-3}$ . For such high temperatures and neutron densities, previous studies have shown that  $(n, \gamma) \rightleftharpoons (\gamma, n)$  equilibrium is achieved (e.g., [29]). In this equilibrium, the abundance distribution in each isotopic chain at a specific proton number  $Z$  is almost strongly peaked at one nucleus. This is referred to as a waiting-point (WP) nucleus because upon reaching it, the  $r$ -process must wait for it to  $\beta$ -decay before producing heavier nuclei. Under this so-called WP approximation, the  $r$ -process path is defined by all the WP nuclei heavier than the seed nuclei, and the progress along this path is regulated by the  $\beta$ -decay of these WP nuclei. So long as this approximation is valid, there is no need to follow neutron capture and photo-disintegration reactions, which

greatly simplifies the  $r$ -process calculation.

Due to the equilibrium between neutron capture and photo-disintegration reactions, the abundance ratio between two neighboring isotopes is given by the Saha equation (e.g., [3–5]):

$$\frac{Y(Z, A+1)}{Y(Z, A)} = n_n \left( \frac{2\pi\hbar^2}{m_u kT} \right)^{\frac{3}{2}} \frac{G(Z, A+1)}{2G(Z, A)} \left( \frac{A+1}{A} \right)^{\frac{3}{2}} \exp \left[ \frac{S_n(Z, A+1)}{kT} \right], \quad (1)$$

where  $\hbar$  is the Planck constant,  $m_u$  is the atomic mass unit,  $k$  is the Boltzmann constant,  $(Z, A)$  indicates a nucleus with proton number  $Z$  and mass number  $A$ , and  $Y$ ,  $G$ , and  $S_n$  denote the number abundance, partition function, and neutron separation energy of the appropriate nucleus, respectively. For a specific isotopic chain, the corresponding WP nucleus has the largest abundance and is determined by the partition functions and neutron separation energies of the relevant nuclei for fixed  $T$  and  $n_n$ . As can be seen from the exponential dependence on the neutron separation energy in Eq. (1), nuclear masses are among the most important input for modeling the  $r$ -process. The other crucial input is  $\beta$ -decay lifetimes of the relevant nuclei.

Over the past two decades, tremendous progress has been made in measuring nuclear properties relevant for the  $r$ -process. For example, the  $\beta$ -decay half-lives of 38 very neutron-rich isotopes bordering the  $r$ -process path have been measured recently [30]. In addition, the masses of a group of nuclei including  $^{80}\text{Zn}$  [31, 32] and  $^{130}\text{Cd}$  [33] have been measured with a very high accuracy [34]. Meanwhile, considerable advance has been made in the theoretical investigation of nuclear masses. The four nuclear mass models used in this paper span from the macroscopic-microscopic kind, represented by the finite-range droplet model (FRDM) [35] and a more recent Weizsäcker-Skyrme (WS\*) model [36], to the microscopic kind, represented by the Skyrme-Hartree-Fock-Bogolyubov mean-field (HFB-17) model [37] and the relativistic mean-field (RMF) model [38]. These models can reproduce the experimentally known neutron separation energies with a root-mean-square deviation of 0.399 (FRDM), 0.332 (WS\*), 0.506 (HFB-17), and 0.653 (RMF) MeV, respectively.

Based on the above overview, there are two frontiers of  $r$ -process research: one focusing on the search for the astrophysical sites and quantification of the conditions therein and the other on acquiring a reliable database for the relevant nuclear input. Observations of elemental abundances in metal-poor stars of the Milky Way halo (see [39] for a review) have shed important light on the  $r$ -process sites (e.g., [40, 41]). The observed  $r$ -patterns also provide an important test of the basic soundness of the nuclear input (e.g., [42]). Of course,

the astrophysical and the nuclear input must be coupled together in order to produce an  $r$ -pattern for comparison with observations. With substantial uncertainties in the current understanding of both the  $r$ -process sites and the nuclear input, parametrization of the astrophysical conditions is often used in exploring the effects of nuclear input on the  $r$ -process production (e.g., [28, 42]). As a practical matter, we adopt the classical approach of using  $T$ ,  $n_n$ , and the corresponding neutron irradiation time  $\tau$  along with the WP approximation (e.g., [43]) to carry out our  $r$ -process calculations below. Our main purpose is to explore the effects of the four nuclear mass models mentioned above on the  $T$  and  $n_n$  conditions required for  $r$ -process nucleosynthesis.

We give a detailed discussion of the WP approximation in Sec. II. Using this approximation along with four nuclear mass models, we derive for each model the  $T$  and  $n_n$  conditions that are required for producing the abundance peaks at  $A \sim 80$ , 130, and 195 as observed in the solar system. In Sec. III we describe the classical approach to simulate the  $r$ -process and use this approach to determine the sets of conditions that can best reproduce the solar  $r$ -pattern and the  $r$ -patterns observed in metal-poor stars for each of the adopted nuclear mass models. We discuss our results and give conclusions in Sec. IV.

## II. $r$ -PROCESS CONDITIONS UNDER THE WP APPROXIMATION

While there are substantial uncertainties in both the  $r$ -process sites and the relevant nuclear input, an essential feature of the  $r$ -process is considered robust: the observed abundance peaks at  $A \sim 80$ , 130, and 195 correspond to the intrinsic properties of extremely neutron-rich nuclei with  $N = 50$ , 82, and 126 closed neutron shells that are produced in the  $r$ -process. As discussed in Sec. I, when  $(n, \gamma) \rightleftharpoons (\gamma, n)$  equilibrium is achieved, the total abundance of an isotopic chain is concentrated in the corresponding WP nucleus. The  $\beta$ -decay lifetimes of the WP nuclei then regulate the abundance pattern resulting from an  $r$ -process episode. In particular, the much longer  $\beta$ -decay lifetimes of extremely neutron-rich nuclei with closed neutron shells than those without produce peaks in  $r$ -patterns. Consequently, in order to produce the observed peaks in  $r$ -patterns under the WP approximation, nuclei with  $N = 50$ , 82, and 126 closed neutron shells and with  $A \sim 80$ , 130, and 195, respectively, must be among the WP nuclei. These critical WP (CWP) nuclei were identified by earlier studies (e.g., [44]). Table I lists the CWP nuclei in the present work. These nuclei

are selected by referring also to previous  $r$ -process calculations [44]. Below we follow the spirit of these studies to derive the conditions required for  $r$ -process nucleosynthesis under the WP approximation by considering the properties of the CWP nuclei.

TABLE I: Critical waiting-point (CWP) nuclei

$N$	CWP nuclei
50	$^{80}\text{Zn}$ , $^{79}\text{Cu}$ , $^{78}\text{Ni}$
82	$^{130}\text{Cd}$ , $^{129}\text{Ag}$ , $^{128}\text{Pd}$ , $^{127}\text{Rh}$ , $^{126}\text{Ru}$
126	$^{195}\text{Tm}$ , $^{194}\text{Er}$ , $^{193}\text{Ho}$ , $^{192}\text{Dy}$ , $^{191}\text{Tb}$

#### A. Role of neutron separation energies

To be quantitative, we define a WP nucleus  $(Z, A_{\text{WP}})$  as one that has an abundance

$$Y(Z, A_{\text{WP}}) \geq 0.5 \sum_A Y(Z, A), \quad (2)$$

where the sum over  $A$  gives the total abundance of the corresponding isotopic chain. For specific  $T$  and  $n_n$ , we can use the above criterion and the relative abundance  $Y(Z, A+1)/Y(Z, A)$  given by Eq. (1) to determine  $(Z, A_{\text{WP}})$  from the nuclear partition functions and neutron separation energies provided by a model. Conversely, we can also determine the  $T$  and  $n_n$  conditions required by a specific WP nucleus. As can be seen from Eq. (1), the predominant dependence of  $Y(Z, A+1)/Y(Z, A)$  is on the neutron separation energy, which can be calculated from a nuclear mass model. We ignore the small differences in the nuclear partition function and in the mass number and rewrite Eq. (1) as

$$\frac{Y(Z, A+1)}{Y(Z, A)} = \exp \left[ \frac{S_n(Z, A+1) - S_n^0(T, n_n)}{kT} \right], \quad (3)$$

where

$$S_n^0(T, n_n) \equiv kT \ln \left[ \frac{2}{n_n} \left( \frac{m_u kT}{2\pi\hbar^2} \right)^{3/2} \right] = T_9 \left[ 2.79 + \frac{1.5 \log T_9 - \log(n_n/10^{20} \text{ cm}^{-3})}{5.04} \right] \text{ MeV}. \quad (4)$$

In the second equality of Eq. (4),  $T_9$  is  $T$  in units of  $10^9$  K. Equation (3) is used in the calculations below.

As an example, we adopt the WS\* mass model to calculate the sets of  $T_9$  and  $n_n$  within the ranges  $1 \leq T_9 \leq 3$  and  $10^{20} \leq n_n \leq 10^{30} \text{ cm}^{-3}$  that are required by the  $N = 82$  CWP nuclei. The results are shown in Fig. 1. For a specific  $T_9$ , the values of  $n_n$  between two identical symbols in this figure would allow the corresponding nucleus to have  $\geq 50\%$  of the total abundance of its isotopic chain. In order to accommodate all the  $N = 82$  CWP nuclei, the common range of  $n_n$  for a specific  $T_9$  is bounded from below by  $^{126}\text{Ru}$  (filled circle) and from above by  $^{130}\text{Cd}$  (filled triangle). This range of  $n_n$  changes with  $T_9$  and is shown as the shaded band in Fig. 1. This band represents the  $T_9$ - $n_n$  conditions required by the  $N = 82$  CWP nuclei.

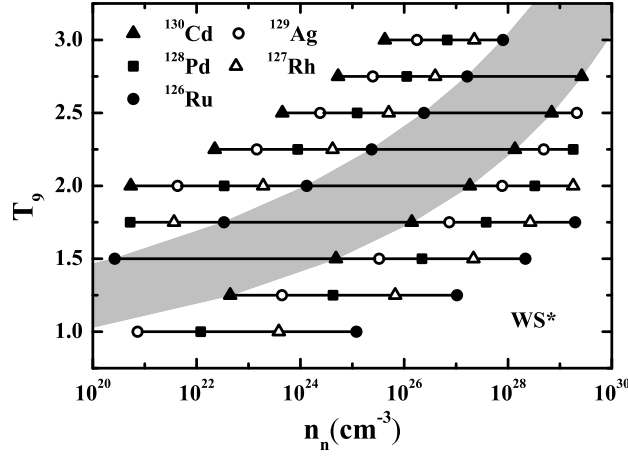


FIG. 1: The  $T_9$ - $n_n$  conditions required by the  $N = 82$  CWP nuclei based on the WS\* mass model. For a specific  $T_9$ , the values of  $n_n$  between two identical symbols would allow the corresponding nucleus to have  $\geq 50\%$  of the total abundance of its isotopic chain. The conditions indicated by the shaded band are required to accommodate all the  $N = 82$  CWP nuclei.

While the neutron separation energies of a large number of nuclei from the WS\* mass model are used in the above calculations, the results in Fig. 1 are determined effectively by the two-neutron separation energies of the  $N = 82$  CWP nuclei and their  $N = 84$  isotopes due to nuclear systematics. This can be understood as follows. Because of the effect of pairing on neutron binding, all WP nuclei have even  $N$ . The relative abundance of two



neighboring even- $N$  isotopes can be obtained from Eq. (3) as

$$\frac{Y(Z, A)}{Y(Z, A - 2)} = \exp \left[ \frac{S_{2n}(Z, A) - 2S_n^0(T, n_n)}{kT} \right], \quad (5)$$

where  $S_{2n}$  denotes the two-neutron separation energy. The values of  $S_{2n}/2$  for isotopes of Ru, Rh, Pd, Ag, and Cd ( $44 \leq Z \leq 48$ ) are shown as functions of  $N$  in Fig. 2, which exhibits the general trend that  $S_{2n}$  essentially monotonically decreases with  $N$  for a specific isotopic chain. Based on this aspect of nuclear systematics, it can be seen from Eq. (5) that the abundance of an even- $N$  isotope increases with  $N$  [ $Y(Z, A)/Y(Z, A - 2) > 1$ ] until  $S_{2n}(Z, A)/2$  falls below  $S_n^0(T, n_n)$ , from which point on it decreases with  $N$  [ $Y(Z, A)/Y(Z, A - 2) < 1$ ]. Therefore, the abundance of even- $N$  isotopes peaks at the nucleus  $(Z, A_{\text{WP}})$ , for which

$$S_{2n}(Z, A_{\text{WP}} + 2) \leq S_n^0(T, n_n) \leq S_{2n}(Z, A_{\text{WP}}). \quad (6)$$

The above equation effectively defines a WP nucleus (e.g., [45]) and can be used to determine the  $T_9$ - $n_n$  conditions required by a specific WP nucleus. For example,  $^{130}\text{Cd}$  has  $S_{2n}/2 = 5.488$  MeV while  $^{132}\text{Cd}$  has  $S_{2n}/2 = 2.869$  MeV [36]. So the  $T_9$ - $n_n$  conditions corresponding to  $2.869 \leq S_n^0(T, n_n) \leq 5.488$  MeV [the band between dashed lines labeled as  $S_n^0(\text{Cd})$  in Fig. 2] are required for  $^{130}\text{Cd}$  to be a WP nucleus. Likewise, the shaded band labeled as  $S_n^0$  in Fig. 2 corresponds to the conditions required to accommodate all the  $N = 82$  CWP nuclei (shaded band in Fig. 1).

### B. $T_9$ - $n_n$ conditions for four nuclear mass models

The calculations in Sec. II A can be generalized to determine the  $T_9$ - $n_n$  conditions required by the  $N = 50$ , 82, and 126 CWP nuclei, respectively, for any specific nuclear mass model. The results for the  $N = 50$  CWP nuclei are presented for the FRDM, WS\*, and RMF models in Fig. 3a, which clearly show that the required conditions change with models. Similar to the case of the  $N = 82$  CWP nuclei (Figs. 1 and 2) discussed in Sec. II A, the upper curve for each model in Fig. 3a is effectively determined by the two-neutron separation energy of the lightest  $N = 50$  CWP nucleus  $^{78}\text{Ni}$  and the lower curve by that of the  $N = 52$  isotope  $^{82}\text{Zn}$  of the heaviest  $N = 50$  CWP nucleus  $^{80}\text{Zn}$ . Therefore, the large differences among the conditions required by the  $N = 50$  CWP nuclei for different models can be traced to the differences in the two-neutron separation energies of  $^{78}\text{Ni}$  and  $^{82}\text{Zn}$  provided by these models.

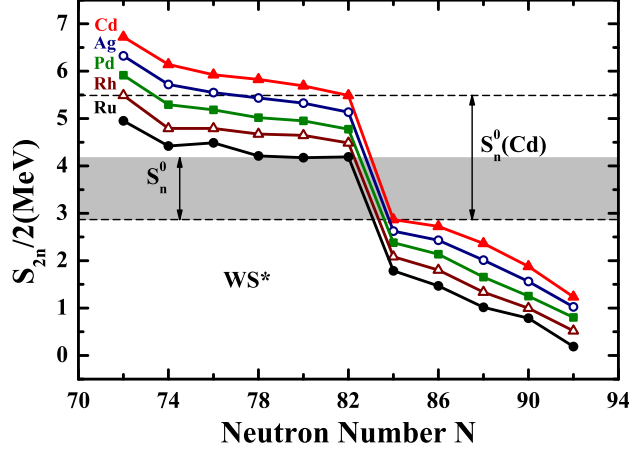


FIG. 2: (Color online) Two-neutron separation energies  $S_{2n}$  for even- $N$  isotopes of Ru, Rh, Pd, Ag, and Cd ( $44 \leq Z \leq 48$ ) in the WS\* model shown in terms of  $S_{2n}/2$  as a function of  $N$  around  $N = 82$ . The band between the dashed lines labeled as  $S_n^0(\text{Cd})$  corresponds to the  $T_9$ - $n_n$  conditions required for  $^{130}\text{Cd}$  to be a WP nucleus. Likewise, the shaded band labeled as  $S_n^0$  corresponds to the conditions required to accommodate all the  $N = 82$  CWP nuclei (shaded band in Fig. 1). See text for details.

In particular, the differences for  $^{82}\text{Zn}$  among the models appear to be substantially larger than those for  $^{78}\text{Ni}$ . We also note that no conditions can be found to accommodate all the  $N = 50$  CWP nuclei for the HFB-17 model, for which the odd-even effects in the neutron separation energy for Ni, Cu, and Zn isotopes around  $N = 50$  are larger by  $\sim 1$ – $1.5$  MeV than those for the FRDM, WS\*, and RMF models.

Noting that the two-neutron separation energies of  $^{78}\text{Ni}$  and  $^{82}\text{Zn}$  can be calculated from the masses tabulated in the latest atomic mass evaluation AME2011-preview [34], we augment the nuclear mass models by using the tabulated values in AME2011-preview when they are available to replace the corresponding model predictions. Remarkably, all four models, including the HFB-17 model, now give the same conditions required by the  $N = 50$  CWP nuclei as shown in Fig. 3b. We find that the changes between Figs. 3a and 3b are caused dominantly by the use of the tabulated masses of  $^{76}\text{Ni}$  to  $^{78}\text{Ni}$  and  $^{78}\text{Zn}$  to  $^{82}\text{Zn}$ , which confirms the crucial roles of the two-neutron separation energies of  $^{78}\text{Ni}$  and  $^{82}\text{Zn}$  in determining the conditions required by the  $N = 50$  CWP nuclei. In the calculations below, we use the FRDM, WS\*, HFB-17, and RMF models that are augmented by AME2011-preview.

We calculate the conditions required by the  $N = 82$  and 126 CWP nuclei, respectively,

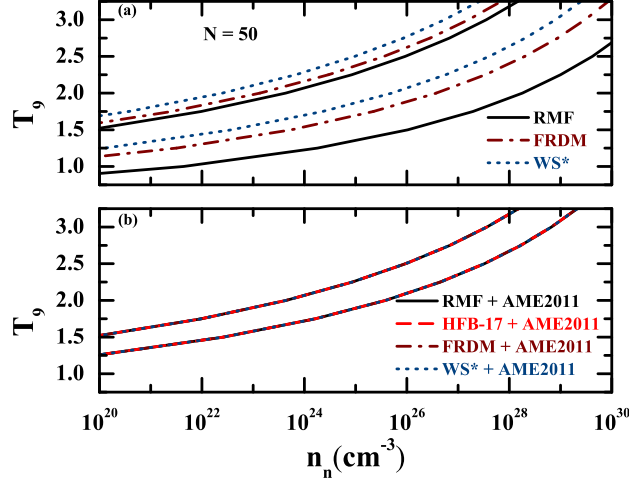


FIG. 3: (Color online) The  $T_9$ - $n_n$  conditions required by the  $N = 50$  CWP nuclei. (a) The band between two curves of the same kind represents the required conditions based on the corresponding mass model. Note the large differences among the results for the three indicated models. Note also that no conditions can be found to accommodate all the  $N = 50$  CWP nuclei based on the HFB-17 model. (b) Same as (a), but for those nuclei the masses of which are tabulated in the latest atomic mass evaluation AME2011-preview [34], the model predictions are replaced by the tabulated values. All four models now give the same conditions required by the  $N = 50$  CWP nuclei.

as in the case of the  $N = 50$  CWP nuclei. The results are summarized in Fig. 4. It can be seen that the conditions required by the  $N = 82$  CWP nuclei (shaded band) are essentially converged for the four augmented nuclear mass models just like those required by the  $N = 50$  CWP nuclei (horizontally hatched band between solid curves). In contrast, the conditions required by the  $N = 126$  CWP nuclei (vertically hatched band between dashed curves) are still strongly dependent on models. This is because these nuclei and the majority of those in the nearby region of the nuclear chart are still out of the reach of experiments while theoretical predictions for their masses involve dramatic extrapolations with large uncertainties (e.g., [32]).

Figure 4 resembles a phase diagram in terms of three bands for the production of the peaks at  $A \sim 80$ , 130, and 195 in  $r$ -patterns that correspond to the  $N = 50$ , 82, and 126 CWP nuclei. For the  $T_9$ - $n_n$  conditions inside the non-overlap region of a band, only a single peak can be produced. For those conditions inside the overlap region of two bands, it is

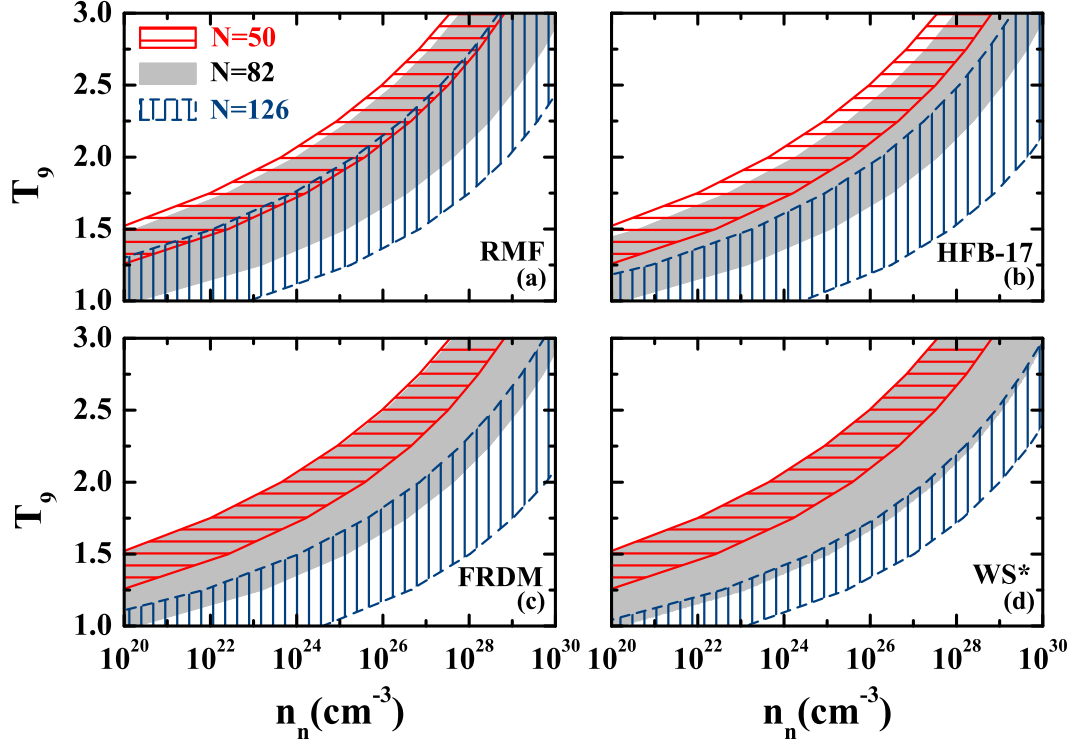


FIG. 4: (Color online) The  $T_9$ - $n_n$  conditions required by the  $N = 50$  (horizontally hatched band between solid curves), 82 (shaded band), and 126 (vertically hatched band between dashed curves) CWP nuclei, respectively, for four nuclear mass models: (a) RMF, (b) HFB-17, (c) FRDM, and (d) WS\*. See text for details.

possible to produce two peaks simultaneously. For the RMF model only, there is a very thin sliver where three bands overlap. Consequently, we consider it very unlikely that three peaks can be produced simultaneously. A close examination of Fig. 4 shows that the  $T_9$ - $n_n$  conditions required by the  $N = 50$  CWP nuclei (horizontally hatched band between solid curves) are distinct from those required by the  $N = 126$  CWP nuclei (vertically hatched band between dashed curves) for the FRDM, HFB-17, and WS\* models. These two sets of conditions overlap only slightly for the RMF model. This suggests that the peaks at  $A \sim 80$  and 195 in  $r$ -patterns are not produced simultaneously. Their production may differ in the time of occurrence within the same astrophysical site or in the astrophysical site itself. In contrast, there is large overlap between the conditions required by the  $N = 50$  and 82 CWP nuclei (shaded band) for the four models considered. In addition, there is slight to significant overlap between the conditions required by the  $N = 82$  and 126 CWP nuclei for

all the models. Therefore, it is possible to produce the peaks at  $A \sim 80$  and 130 or those at  $A \sim 130$  and 195 simultaneously. The above results will be examined by detailed  $r$ -process calculations in Sec. III.

### III. $r$ -PATTERNS FROM THE CLASSICAL APPROACH

Our main goal here is to explore the effects of nuclear masses on the conditions required for  $r$ -process nucleosynthesis under the WP approximation. As discussed in Sec. II, these conditions are mostly set by the neutron separation energies, which we calculate from four nuclear mass models augmented by the latest atomic mass evaluation AME2011-preview. As confirmation of these results, we calculate the  $r$ -patterns produced under the conditions shown in Fig. 4 and compare them with those inferred for the solar system and observed in metal-poor stars. As the range of conditions shown in Fig. 4 is rather broad, we sample these conditions at a fixed temperature. Specifically, we use  $T_9 = 1.5$  and  $n_n = 10^{20.0}$ – $10^{22.5}$ ,  $10^{20.5}$ – $10^{25.0}$ , and  $10^{23.5}$ – $10^{27.5}$   $\text{cm}^{-3}$  as typical conditions required by the  $N = 50$ , 82, and 126 CWP nuclei, respectively. As noted in Sec. IIB, there is overlap between these sets of conditions, which can lead to coproduction of two peaks in the  $r$ -pattern.

We carry out an  $r$ -process calculation using the classical approach (e.g., [3–5]) as follows. We take the seed nucleus to be  $^{56}\text{Fe}$  ( $Z = 26$ ). We assume that some material with an initial abundance  $Y_{\text{Fe}}$  of  $^{56}\text{Fe}$  is irradiated with neutrons at fixed  $T$  and  $n_n$  for a time  $\tau$ . We then use Eq. (3) along with a nuclear mass model to calculate the fractional abundance  $P(Z, A)$  for all the nuclei in each of the isotopic chains with  $Z \geq 26$ , where

$$P(Z, A) \equiv \frac{Y(Z, A)}{\sum_A Y(Z, A)}. \quad (7)$$

Note that for fixed  $T$  and  $n_n$ ,  $P(Z, A)$  is also fixed. Using the fractional abundances, we calculate the effective  $\beta$ -decay rate of an isotopic chain as

$$\lambda_{\beta, Z} \equiv \sum_A P(Z, A) \lambda_{\beta}(Z, A), \quad (8)$$

where  $\lambda_{\beta}(Z, A)$  is the  $\beta$ -decay rate of the nucleus  $(Z, A)$ . For all our calculations, we use  $\lambda_{\beta}(Z, A)$  from the experimental data in Ref. [46] for the nuclei with measurements and from the theoretical estimates in Ref. [47] based on the FRDM+QRPA method for those without. We then solve the set of equations

$$\dot{Y}_Z(t) = -\lambda_{\beta, Z} Y_Z(t), \quad Z = 26, \quad (9)$$

$$\dot{Y}_Z(t) = \lambda_{\beta,Z-1}Y_{Z-1}(t) - \lambda_{\beta,Z}Y_Z(t), \quad Z > 26, \quad (10)$$

where the dot denotes the derivative with respect to time  $t$ , and  $Y_Z(t)$  is the total abundance of the isotopic chain with proton number  $Z$  at time  $t$ . The initial conditions are  $Y_Z(0) = Y_{\text{Fe}}$  for  $Z = 26$  and 0 for  $Z > 26$ . We assume that the  $r$ -process freezes out instantaneously at  $t = \tau$ . The freeze-out abundance of the nucleus  $(Z, A)$  is

$$Y_{\text{fo}}(Z, A) = P(Z, A)Y_Z(\tau). \quad (11)$$

The final abundance distribution from an  $r$ -process episode is obtained by following the  $\beta$  and  $\alpha$  decays of all the nuclei in the freeze-out distribution. We include  $\beta$ -delayed emission of up to three neutrons [47], which has the important effect of smoothing the final  $r$ -pattern. The data on  $\alpha$ -decays are taken from the National Nuclear Data Center [48]. Fission is ignored in all the calculations. Note that the WP approximation is implicit in the classical approach as  $Y_Z(t)$  is dominated by the corresponding WP nucleus with  $P(Z, A_{\text{WP}}) \geq 0.5$ .

For comparison with the  $r$ -patterns inferred for the solar system and observed in metal-poor stars, we need to superpose the results from many  $r$ -process episodes described above. As we take  $T_9 = 1.5$  for all the calculations, we denote each episode by its  $n_n$ . The neutron irradiation time  $\tau(n_n)$  and the weight  $\omega(n_n)$  for each episode are taken to be

$$\tau(n_n) = a \times n_n^b, \quad (12)$$

$$\omega(n_n) = c \times n_n^d, \quad (13)$$

where  $a, b, c$ , and  $d$  are parameters to be determined by a least-squares fit to the  $r$ -pattern used for comparison. The above procedure has been used extensively in  $r$ -process studies (e.g., [28, 43, 49–52]).

### A. Comparison with solar-like $r$ -patterns

We first use the classical approach to reproduce the solar  $r$ -pattern for  $125 \leq A \leq 209$  [53] (see also e.g., [51, 54]), which is shown as the dashed curve in Fig. 5. We consider a superposition of nine neutron densities (equidistant on log scale) within the range  $10^{23.5} \leq n_n \leq 10^{27.5} \text{ cm}^{-3}$ , which corresponds to the typical conditions required by the  $N = 126$  CWP nuclei for  $T_9 = 1.5$  (see Fig. 4). The best-fit results (hereafter “Fit I”) for the four

adopted nuclear mass models are shown as the solid curves in Fig. 5. Note that although the fits are performed for the solar isotopic  $r$ -pattern, the patterns shown in Fig. 5 are for the corresponding elemental abundances. It can be seen that the solar  $r$ -pattern from the peak at  $A \sim 130$  ( $Z \sim 52$ , Te) to that at  $A \sim 195$  ( $Z \sim 78$ , Pt) is reproduced rather well for the FRDM, HBF-17, and WS\* models. For the RMF model, the rare-earth elements with  $Z = 66\text{--}70$  (Dy, Ho, Er, Tm, Yb) are severely underproduced. This deficiency may reflect the necessity to adopt improved RMF parameter sets (e.g., PC-PK1 [55] which provides much better descriptions for the nuclear ground-state and excited state properties [56]) or that the classical approach is inadequate to give a full description of  $r$ -process nucleosynthesis (e.g., instantaneous freeze-out is not a good approximation [28]). In any case, the peaks at  $A \sim 130$  and 195 are reproduced adequately for all four mass models, which suggests that the typical conditions required by the  $N = 126$  CWP nuclei can indeed produce both these peaks. As discussed in Sec. II B, this is because there is significant overlap between the conditions required by the  $N = 82$  and 126 CWP nuclei (see Fig. 4).

Observations show that Ba ( $Z = 56$ ) and heavier elements in many metal-poor stars of the Milky Way halo follow the solar  $r$ -pattern rather closely [39]. The values of  $\log \varepsilon(E) \equiv \log(E/H) + 12$  for the elements with  $38 \leq Z \leq 79$  obtained by averaging the data [39, 54, 57, 58] on two such “ $r$ -II” stars, CS 22892–052 and CS 31082–001, are shown as filled circles in Fig. 5. The data on Pb ( $Z = 82$ ) and Th ( $Z = 90$ ) for CS 22892–052 are also shown. The solar  $r$ -pattern has been translated to pass through the data on Eu ( $Z = 63$ ) and can be seen to represent the pattern for  $Z \geq 56$  in  $r$ -II stars very well. Recently, Te ( $Z = 52$ ) has been measured in a group of metal-poor stars (BD +17°3248, HD 108317, HD 128279 [59]; HD 160617 [60]). This extends the comparison of  $r$ -patterns in metal-poor stars with the solar  $r$ -pattern to include an element in the peak at  $A \sim 130$ . The data on Te for BD +17°3248 (shifted according to the observed Te/Eu ratio) is shown as the filled square in Fig. 5. It can be seen that the Te data is consistent with the solar  $r$ -pattern and with the coproduction of the peaks at  $A \sim 130$  and 195 under the typical conditions required by the  $N = 126$  CWP nuclei. The above results are also in agreement with previous studies (e.g., [49, 51]), which concluded that the  $r$ -process responsible for the elements with  $56 \leq Z \leq 82$  is characterized by neutron densities of  $10^{23}\text{--}10^{28} \text{ cm}^{-3}$ .

The Fit I results shown in Fig. 5 cannot adequately reproduce the abundances of the elements with  $38 \leq Z \leq 47$  in  $r$ -II stars (especially when the RMF model is used). Further,

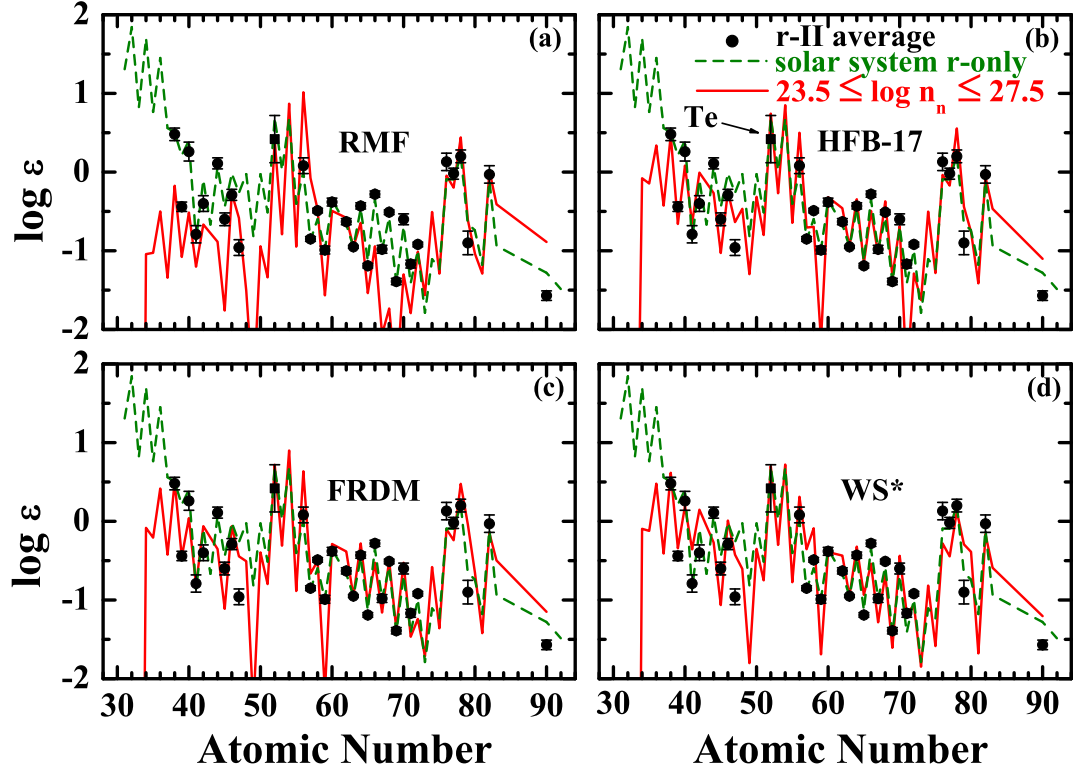


FIG. 5: (Color online) Elemental abundances (solid curves) calculated from the classical  $r$ -process approach using four nuclear mass models: (a) RMF, (b) HFB-17, (c) FRDM, and (d) WS\*. The filled circles represent the average data on  $r$ -II stars of the Milky Way halo and the dashed curve is the solar  $r$ -pattern translated to pass through the Eu data. The filled square gives the Te abundance recently measured in the metal-poor star BD +17°3248 (shifted according to the observed Te/Eu ratio). The calculated solid curves (Fit I) are the best-fit results to reproduce the solar isotopic  $r$ -pattern for  $125 \leq A \leq 209$  with  $T_9 = 1.5$  and  $10^{23.5} \leq n_n \leq 10^{27.5} \text{ cm}^{-3}$ , which are the typical conditions required by the  $N = 126$  CWP nuclei. See text for details.

the elements in the peak at  $A \sim 80$  ( $Z \sim 34$ ) of the solar  $r$ -pattern are severely underproduced by these calculations. Additional  $r$ -process contributions to or alternative sources for the elements below the peak at  $A \sim 130$  are thus required and this issue has been under active investigation [40, 61–64]. Here we explore the possibility that there are additional contributions from  $r$ -process nucleosynthesis under the conditions required by the  $N = 50$  CWP nuclei. We consider a superposition of six neutron densities (equidistant on log scale) within the range  $10^{20.0} \leq n_n \leq 10^{22.5} \text{ cm}^{-3}$  to best reproduce the solar isotopic  $r$ -pattern for  $69 \leq A \leq 124$  (hereafter “Fit II”). The results are shown as the solid curves in Fig. 6. It



can be seen that the conditions required by the  $N = 50$  CWP nuclei indeed can produce the peak at  $A \sim 80$ . However, it is also clear that the  $r$ -patterns from the peak at  $A \sim 130$  to that at  $A \sim 195$  inferred for the solar system and observed in  $r$ -II stars require very different conditions from those for producing the peak at  $A \sim 80$ .

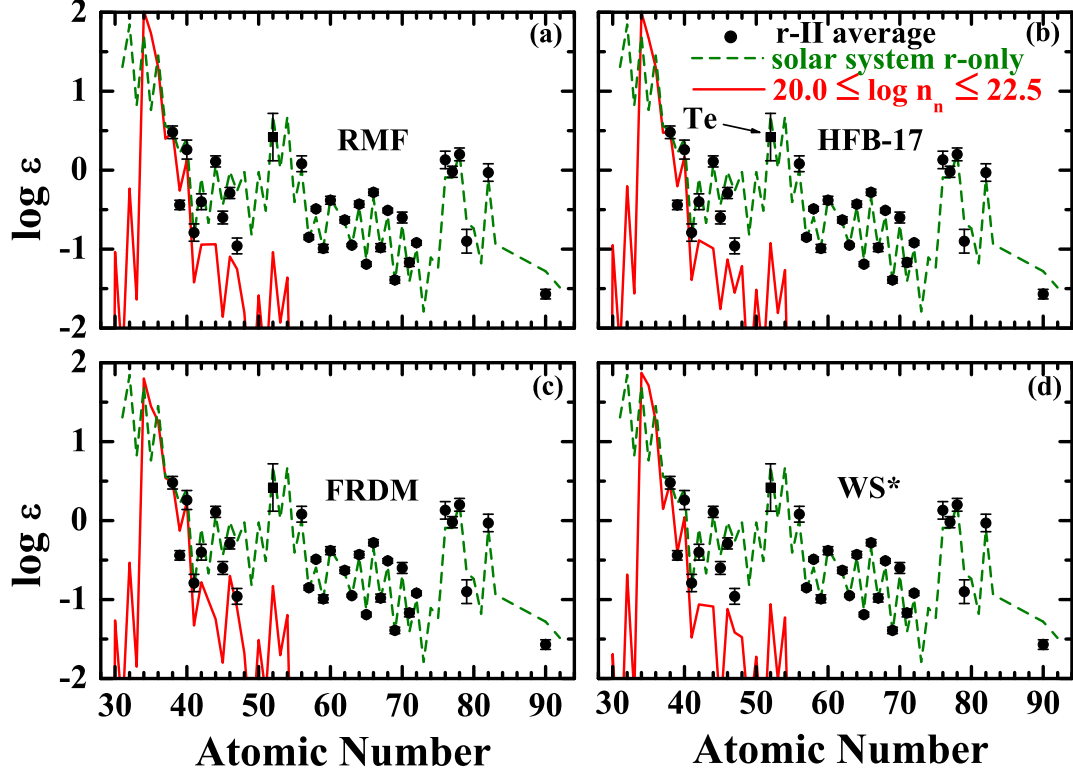


FIG. 6: (Color online) Same as Fig. 5, but the solid curves (Fit II) are the best-fit results to reproduce the solar isotopic  $r$ -pattern for  $69 \leq A \leq 124$  with  $T_9 = 1.5$  and  $10^{20.0} \leq n_n \leq 10^{22.5} \text{ cm}^{-3}$ , which are the typical conditions required by the  $N = 50$  CWP nuclei. See text for details.

To find the best match to the  $r$ -pattern in  $r$ -II stars, we consider a superposition of neutron densities in the two ranges adopted for Fits I and II. The results are shown as the solid curves in Fig. 7. It can be seen that fair agreement between the calculated and observed patterns is obtained for the FRDM, HFB-17, and WS\* models. Note also that the calculated Te abundances (crosses) for all four models are consistent with the newly measured value for the metal-poor star BD +17°3248. However, the trough at  $Z = 66$ –70 is clearly problematic for the RMF model. This may be caused by nuclear shape transition before the  $N = 126$  closed neutron shell and the location of the transition region could have

been assigned incorrectly in the RMF model [50]. Discrepancies can also be seen for Ru, Rh, and Ag ( $Z = 44, 45$ , and  $47$ , respectively) for all four models. This issue needs to be addressed by detailed considerations of the astrophysical environments for the  $r$ -process and alternative sources for the elements below the peak at  $A \sim 130$  [40, 61–64].

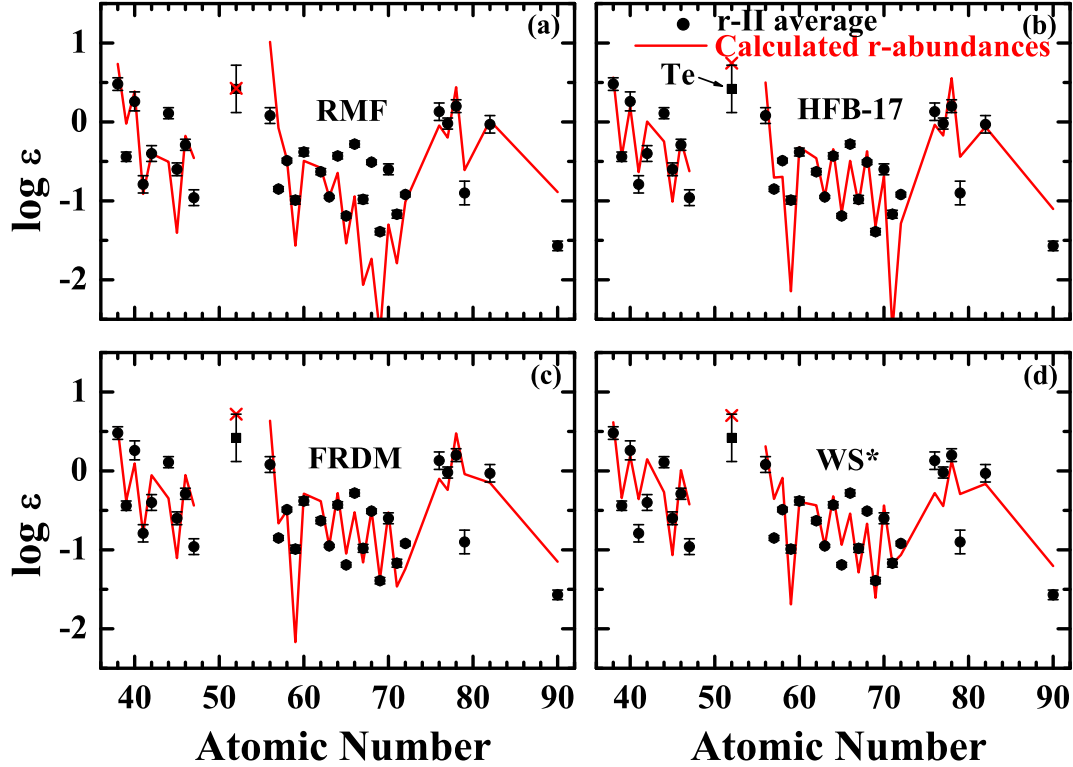


FIG. 7: (Color online) Best fits (solid curves) to the  $r$ -pattern in  $r$ -II stars using a superposition of neutron densities within the ranges  $10^{20.0} \leq n_n \leq 10^{22.5} \text{ cm}^{-3}$  and  $10^{23.5} \leq n_n \leq 10^{27.5} \text{ cm}^{-3}$  for four nuclear mass models: (a) RMF, (b) HFB-17, (c) FRDM, and (d) WS\*. The crosses give the calculated Te abundances, which are consistent with the measure value (filled square) for the metal-poor star BD +17°3248 (shifted according to the observed Te/Eu ratio). See text for details.

## B. Comparison with a non-solar-like $r$ -pattern

In contrast to the  $r$ -II stars, some metal-poor stars exhibit an  $r$ -pattern that is clearly different from the solar one. Prominent examples are the metal-poor stars HD 122563 [65] and HD 88609 [66], which have almost the same abundances for Cu ( $Z = 29$ ) and heavier elements. The data on Sr ( $Z = 38$ ) and heavier elements for HD 122563 are shown as the

filled circles in Fig. 8. Relative to the solar  $r$ -pattern translated to pass through the Eu data (dashed curve), the elements below the peak at  $A \sim 130$  in this star are grossly overabundant while those heavier than Eu are underabundant. It was argued that in addition to an  $r$ -process source for producing a solar-like  $r$ -pattern from the peak at  $A \sim 130$  to that at  $A \sim 195$ , a very different source is required to explain the data for stars like HD 122563 [40, 65, 66].

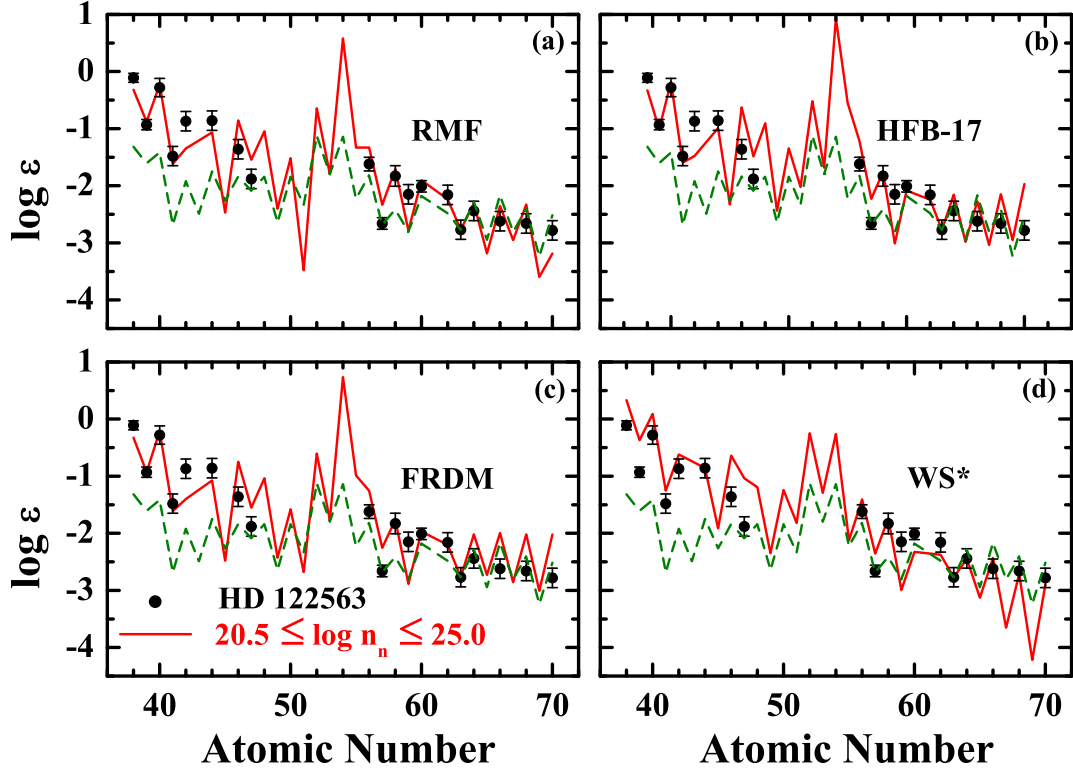


FIG. 8: (Color online) Best fits (solid curves) to the non-solar-like  $r$ -pattern (filled circles) in the metal-poor star HD 122563 for four nuclear mass models: (a) RMF, (b) HFB-17, (c) FRDM, and (d) WS\*. These results use a superposition of neutron densities within the range  $10^{20.5} \leq n_n \leq 10^{25.0} \text{ cm}^{-3}$ , which corresponds to the typical conditions required by the  $N = 82$  CWP nuclei for  $T_9 = 1.5$ . The dashed curve gives the solar  $r$ -pattern translated to pass through the filled circle for Eu ( $Z = 63$ ). See text for details.

Here we attempt to interpret the abundance pattern observed in HD 122563 using the classical  $r$ -process approach. We find that the conditions required by the  $N = 82$  CWP nuclei can best reproduce this pattern while those required by the  $N = 50$  and 126 CWP nuclei can not. The best-fit results use a superposition of ten neutron densities (equidistant

on log scale) within the range  $10^{20.5} \leq n_n \leq 10^{25.0} \text{ cm}^{-3}$ , which corresponds to the typical conditions required by the  $N = 82$  CWP nuclei for  $T_9 = 1.5$  (see Fig. 4). These results are shown as the solid curves in Fig. 8. It can be seen that an approximate overall match of the calculated with the observed abundances is obtained for all four nuclear mass models. Therefore, we suggest that it is plausible to account for the abundance pattern in stars like HD 122563 by an  $r$ -process operating under the conditions required by the  $N = 82$  CWP nuclei. We note that Fig. 8 shows a clear difference in the calculated relative production of Te and Xe ( $Z = 52$  and  $54$ , respectively) between the WS\* and the other three mass models: these two elements are produced in approximately equal amount for the WS\* model but Xe is produced much more than Te for the other three models. Measurements of these two elements in HD 122563 would be extremely valuable in constraining nuclear mass models although they also represent a difficult challenge to spectroscopic observations.

#### IV. DISCUSSION AND CONCLUSIONS

We have explored the effects of four nuclear mass models (FRDM, WS\*, HFB-17, and RMF) on the conditions required by  $r$ -process nucleosynthesis under the WP approximation. As discussed in Sec. II, the required  $T_9$ - $n_n$  conditions are mostly determined by the two-neutron separation energies of the CWP nuclei with  $N = 50, 82$ , and  $126$  and of those nuclei around them. Figure 3 shows the dramatic effect of using the tabulated values in the latest atomic mass evaluation AME2011-preview when they are available to replace the masses predicted by models. As noted in Sec. IIB, the tabulated masses of  $^{76}\text{Ni}$  to  $^{78}\text{Ni}$  and  $^{78}\text{Zn}$  to  $^{82}\text{Zn}$  play crucial roles in determining the conditions required by the  $N = 50$  CWP nuclei. However, the tabulated masses of  $^{76}\text{Ni}$  to  $^{78}\text{Ni}$  and  $^{82}\text{Zn}$  are extrapolated rather than measured. To emphasize the effects of these masses on the conditions required by the  $N = 50$  CWP nuclei, we first repeat the calculations of Sec. II by varying the neutron separation energy of  $^{78}\text{Ni}$  within the estimated uncertainty of  $0.946 \text{ MeV}$  [34] while keeping the other input the same as for Fig. 3b. The results are shown in Fig. 9a. In comparison with Fig. 3b, the lower bound on the region of the required  $T_9$ - $n_n$  conditions stays the same because this is determined by the two-neutron separation energy of  $^{82}\text{Zn}$  (see Sec. IIB), which is not changed. Increasing the neutron separation energy of  $^{78}\text{Ni}$  by  $0.946 \text{ MeV}$  raises the upper bound from the solid curve (upper bound in Fig. 3b) to

the dashed curve and decreasing this quantity by the same amount lowers it to the dotted curve. We then repeat the same calculations but vary the neutron separation energy of  $^{82}\text{Zn}$  within the estimated uncertainty of 0.401 MeV [34]. The effects on the lower bound on the region of the required  $T_9$ - $n_n$  conditions are shown in Fig. 9b. Note that if the neutron separation energy of  $^{78}\text{Ni}$  were lower than its tabulated value by 0.946 MeV while that of  $^{82}\text{Zn}$  were higher by 0.401 MeV, then it would be almost impossible to find any  $T_9$ - $n_n$  conditions to accommodate all the  $N = 50$  CWP nuclei. In any case, the significant effects of uncertainties in neutron separation energies on the required  $T_9$ - $n_n$  conditions shown in Fig. 9 clearly demonstrate the importance of precise mass measurements for  $^{76}\text{Ni}$  to  $^{78}\text{Ni}$  and  $^{82}\text{Zn}$ .

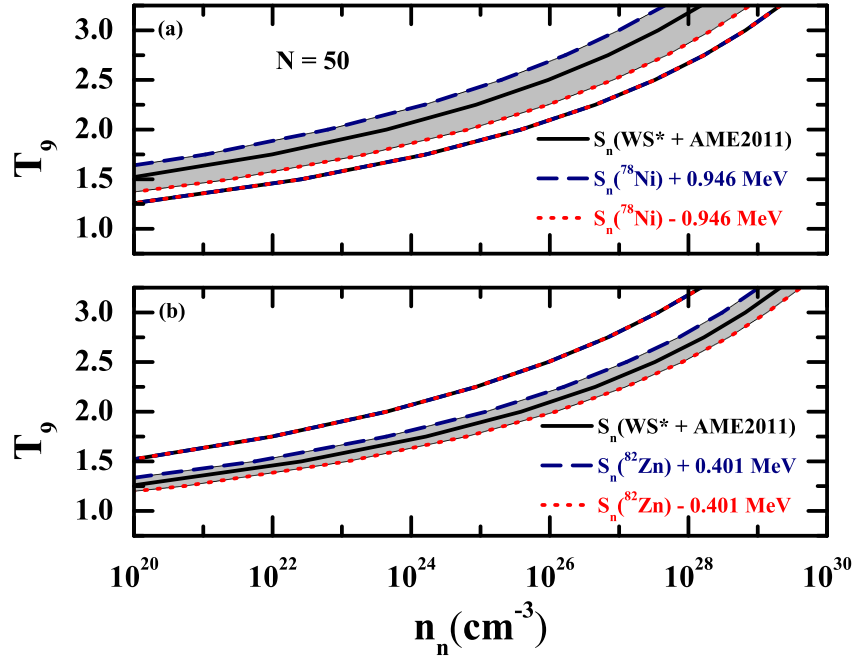


FIG. 9: (Color online) Effects of the uncertainty in the neutron separation energy  $S_n$  for (a)  $^{78}\text{Ni}$  and (b)  $^{82}\text{Zn}$  on the  $T_9$ - $n_n$  conditions required by the  $N = 50$  CWP nuclei. The solid curves are the same as those in Fig. 3b. The shaded regions show the effects on the required  $T_9$ - $n_n$  conditions when the corresponding  $S_n$  values are varied within the estimated uncertainties. See text for details.

As in the case of  $N = 50$  CWP nuclei, we have also made a careful scan of the nuclear chart around the  $N = 82$  CWP nuclei and explored the effects of those nuclei with experimentally unknown or poorly measured masses on the  $T_9$ - $n_n$  conditions required by the  $N = 82$  CWP

nuclei. When nuclear masses are not known experimentally, we have used the extrapolated masses and uncertainties as these have been proven to have a better predictive power than all available models [67, 68]. We have identified  $^{131}\text{Cd}$  and  $^{132}\text{Cd}$  as additional key nuclei for precise mass measurements.

In conclusion, we have estimated the temperature and neutron density conditions required for  $r$ -process nucleosynthesis under the WP approximation using four nuclear mass models augmented by the latest atomic mass evaluation AME2011-preview. We have shown that these conditions are mostly determined by the two-neutron separation energies of the  $N = 50, 82$ , and  $126$  CWP nuclei and those around them. We have also identified some key nuclei including  $^{76}\text{Ni}$  to  $^{78}\text{Ni}$ ,  $^{82}\text{Zn}$ ,  $^{131}\text{Cd}$ , and  $^{132}\text{Cd}$  for precise mass measurements at rare-isotope beam facilities.

Based on the typical conditions required by the  $N = 50, 82$ , and  $126$  CWP nuclei shown in Fig. 4, we have performed  $r$ -process calculations in the classical approach to reproduce the  $r$ -pattern inferred for the solar system and those observed in metal-poor stars of the Milky Way halo. We have found that (1) the conditions required to produce the peak at  $A \sim 80$  differ greatly from those required to produce the solar  $r$ -pattern from the peak at  $A \sim 130$  to that at  $A \sim 195$ , which reflects that the  $T_9$ - $n_n$  conditions required by the  $N = 50$  and  $126$  CWP nuclei are very different; (2) the solar  $r$ -pattern from the peak at  $A \sim 130$  to that at  $A \sim 195$ , which also closely describes the  $r$ -patterns in many metal-poor stars, can be reproduced under the conditions required by the  $N = 126$  CWP nuclei, which has significant overlap with those required by the  $N = 82$  CWP nuclei, thereby enabling coproduction of the peaks at  $A \sim 130$  and  $195$ ; (3) it is plausible to explain the overall  $r$ -patterns in metal-poor  $r$ -II stars with a superposition of two sets of  $r$ -process conditions required by the  $N = 50$  and  $126$  CWP nuclei, respectively; and (4) the non-solar-like  $r$ -pattern observed in metal-poor stars like HD 122563 can be accounted for by the  $r$ -process conditions required by the  $N = 82$  CWP nuclei.

We recognize that the classical  $r$ -process approach leaves out many important details, such as the time evolution of temperature and neutron density, the finite duration of the freeze-out, and the breakdown of  $(n, \gamma) \rightleftharpoons (\gamma, n)$  equilibrium during the freeze-out. However, it is very likely that the conditions derived here are valid approximation to those obtained immediately before the freeze-out in hot  $r$ -process environments where  $(n, \gamma) \rightleftharpoons (\gamma, n)$  equilibrium can be achieved. We intend to carry out parametric studies of the  $r$ -process based

on more detailed and more realistic astrophysical models in the future, and will explore the effects of various nuclear input on such models.

## Acknowledgments

This work was supported in part by the 973 Program (No. 2007CB815000), the National Natural Science Foundation of China (Nos. 10975007, 10975008, 11005069, 11035007, 11105010, 11128510, and 11175002), the Research Fund for the Doctoral Program of Higher Education (No. 20110001110087), the Program for New Century Excellent Talents in University (No. NCET-09-0031), and the 211 Project of Anhui University (No. 02303319) in the People's Republic of China, and by the US DOE under DE-FG02-87ER40328 at the University of Minnesota.

- 
- [1] E. M. Burbidge, G. R. Burbidge, W. A. Fowler, and F. Hoyle, *Rev. Mod. Phys.* **29**, 547 (1957).
  - [2] A. G. W. Cameron, Chalk River Report **CRL-41** (1957).
  - [3] J. J. Cowan, F.-K. Thielemann, and J. W. Truran, *Phys. Rep.* **208**, 267 (1991).
  - [4] Y.-Z. Qian, *Prog. Part. Nucl. Phys.* **50**, 153 (2003).
  - [5] M. Arnould, S. Goriely, and K. Takahashi, *Phys. Rep.* **450**, 97 (2007).
  - [6] F. Käppeler, R. Gallino, S. Bisterzo, and W. Aoki, *Rev. Mod. Phys.* **83**, 157 (2011).
  - [7] S. E. Woosley and R. D. Hoffman, *Astrophys. J.* **395**, 202 (1992).
  - [8] B. S. Meyer, G. J. Mathews, W. M. Howard, S. E. Woosley, and R. D. Hoffman, *Astrophys. J.* **399**, 656 (1992).
  - [9] S. E. Woosley, J. R. Wilson, G. J. Mathews, R. D. Hoffman, and B. S. Meyer, *Astrophys. J.* **433**, 229 (1994).
  - [10] H. Ning, Y.-Z. Qian, and B. S. Meyer, *Astrophys. J.* **667**, L159 (2007).
  - [11] J. Pruet, S. E. Woosley, and R. D. Hoffman, *Astrophys. J.* **586**, 1254 (2003).
  - [12] R. Surman, G. C. McLaughlin, and W. R. Hix, *Astrophys. J.* **643**, 1057 (2006).
  - [13] R. Surman, G. C. McLaughlin, M. Ruffert, H.-T. Janka, and W. R. Hix, *Astrophys. J.* **679**, L117 (2008).
  - [14] S. Wanajo and H.-T. Janka, *Astrophys. J.* **746**, 180 (2012).

- [15] R. I. Epstein, S. A. Colgate, and W. C. Haxton, Phys. Rev. Lett. **61**, 2038 (1988).
- [16] P. Banerjee, W. C. Haxton, and Y.-Z. Qian, Phys. Rev. Lett. **106**, 201104 (2011).
- [17] J. M. Lattimer, F. Mackie, D. G. Ravenhall, and D. N. Schramm, Astrophys. J. **213**, 225 (1977).
- [18] C. Freiburghaus, S. Rosswog, and F.-K. Thielemann, Astrophys. J. **525**, L121 (1999).
- [19] S. Goriely, A. Bauswein, and H.-T. Janka, Astrophys. J. **738**, L32 (2011).
- [20] O. Korobkin, S. Rosswog, A. Arcones, and C. Winteler, arXiv:1206.2379.
- [21] H.-T. Janka, arXiv:1206.2503.
- [22] G. Martínez-Pinedo, T. Fischer, A. Lohs, and L. Huther, arXiv:1205.2793.
- [23] L. F. Roberts, and S. Reddy, arXiv:1205.4066.
- [24] Y.-Z. Qian, Astrophys. J. **534**, L67 (2000).
- [25] D. Argast, M. Samland, F.-K. Thielemann, and Y.-Z. Qian, Astron. Astrophys. **416**, 997 (2004).
- [26] E. De Donder and D. Vanbeveren, New Astron. Rev. **48**, 861 (2004).
- [27] D. Page and S. Reddy, Annu. Rev. Nucl. Part. Sci. **56**, 327 (2006).
- [28] C. Freiburghaus, J.-F. Rembges, T. Rauscher, E. Kolbe, F.-K. Thielemann, K.-L. Kratz, B. Pfeiffer, and J. J. Cowan, Astrophys. J. **516**, 381 (1999).
- [29] S. Goriely and M. Arnould, Astron. Astrophys. **312**, 327 (1996).
- [30] S. Nishimura *et al.*, Phys. Rev. Lett. **106**, 052502 (2011).
- [31] S. Baruah *et al.*, Phys. Rev. Lett. **101**, 262501 (2008).
- [32] B. Sun *et al.*, Nucl. Phys. A **812**, 1 (2008).
- [33] I. Dillmann *et al.* (the ISOLDE Collaboration), Phys. Rev. Lett. **91**, 162503 (2003).
- [34] G. Audi and W. Meng, private Communication April 2011, <http://amdc.in2p3.fr/masstable/Ame2011int/file.html>
- [35] P. Möller, J. Nix, W. Myers, and W. Swiatecki, At. Data Nucl. Data Tables **59**, 185 (1995).
- [36] N. Wang, Z. Liang, M. Liu, and X. Wu, Phys. Rev. C **82**, 044304 (2010).
- [37] S. Goriely, N. Chamel, and J. M. Pearson, Phys. Rev. Lett. **102**, 152503 (2009).
- [38] L. Geng, H. Toki, and J. Meng, Prog. Theor. Phys. **113**, 785 (2005).
- [39] C. Sneden, J. J. Cowan, and R. Gallino, Annu. Rev. Astron. Astro. **46**, 241 (2008).
- [40] Y.-Z. Qian and G. Wasserburg, Phys. Rep. **442**, 237 (2007).
- [41] K. Farouqi, K.-L. Kratz, L. I. Mashonkina, B. Pfeiffer, J. J. Cowan, F.-K. Thielemann, and



- J. W. Truran, *Astrophys. J.* **694**, L49 (2009).
- [42] K. Farouqi, K.-L. Kratz, B. Pfeiffer, T. Rauscher, F.-K. Thielemann, and J. W. Truran, *Astrophys. J.* **712**, 1359 (2010).
  - [43] K.-L. Kratz, J. P. Bitouzet, F. K. Thielemann, P. Möller, and B. Pfeiffer, *Astrophys. J.* **403**, 216 (1993).
  - [44] K.-L. Kratz, F. K. Thielemann, W. Willebrandt, P. Möller, V. Harms, A. Wöhr, and J. W. Truran, *J. Phys. G* **14**, S331 (1988).
  - [45] S. Goriely and M. Arnould, *Astron. Astrophys.* **262**, 73 (1992).
  - [46] G. Audi, A. Wapstra, and C. Thibault, *Nucl. Phys. A* **729**, 337 (2003).
  - [47] P. Möller, B. Pfeiffer, and K.-L. Kratz, *Phys. Rev. C* **67**, 055802 (2003).
  - [48] National Nuclear Data Center, <http://www.nndc.bnl.gov>
  - [49] K.-L. Kratz, K. Farouqi, B. Pfeiffer, J. W. Truran, C. Sneden, and J. J. Cowan, *Astrophys. J.* **662**, 39 (2007).
  - [50] B. Sun, F. Montes, L. S. Geng, H. Geissel, Y. A. Litvinov, and J. Meng, *Phys. Rev. C* **78**, 025806 (2008).
  - [51] Z. Niu, B. Sun, and J. Meng, *Phys. Rev. C* **80**, 065806 (2009).
  - [52] Z. Li, Z. M. Niu, B. Sun, N. Wang, and J. Meng, *Acta Phys. Sin.* **61**, 072601 (2012) (in Chinese).
  - [53] J. J. Cowan, J. E. Lawler, C. Sneden, E. A. den Hartog, and J. Collier, in *Proceedings of the 2006 NASA Laboratory Astrophysics Workshop*, NASA/CP-2006-214549, p. 82.
  - [54] C. Sneden et al., *Astrophys. J.* **591**, 936 (2003).
  - [55] P. W. Zhao, Z. P. Li, J. M. Yao, and J. Meng, *Phys. Rev. C* **82**, 054319 (2010).
  - [56] J. Meng, H. Toki, S. G. Zhou, S. Q. Zhang, W. H. Long, and L. S. Geng, *Prog. Part. Nucl. Phys.* **57**, 470 (2006).
  - [57] V. Hill, B. Plez, R. Cayrel, T. C. Beers, B. Nordström, J. Andersen, M. Spite, F. Spite, B. Barbuy, P. Bonifacio, et al., *Astron. Astrophys.* **387**, 560 (2002).
  - [58] C. Sneden, J. E. Lawler, J. J. Cowan, I. I. Ivans, and E. A. D. Hartog, *Astrophys. J. Suppl. Ser.* **182**, 80 (2009).
  - [59] I. U. Roederer, J. E. Lawler, J. J. Cowan, T. C. Beers, A. Frebel, I. I. Ivans, H. Schatz, J. S. Sobeck, and C. Sneden, *Astrophys. J.* **747**, L8 (2012).
  - [60] I. U. Roederer and J. E. Lawler, *Astrophys. J.* **750**, 76 (2012).

- [61] Y.-Z. Qian and G. Wasserburg, *Astrophys. J.* **559**, 925 (2001).
- [62] C. Travaglio, R. Gallino, E. Arnone, J. Cowan, F. Jordan, and C. Sneden, *Astrophys. J.* **601**, 864 (2004).
- [63] Y. Ishimaru, S. Wanajo, W. Aoki, S. G. Ryan, and N. Prantzos, *Nucl. Phys. A* **758**, 603 (2005).
- [64] F. Montes et al., *Astrophys. J.* **671**, 1685 (2007).
- [65] S. Honda, W. Aoki, Y. Ishimaru, S. Wanajo, and S. G. Ryan, *Astrophys. J.* **643**, 1180 (2006).
- [66] S. Honda, W. Aoki, Y. Ishimaru, and S. Wanajo, *Astrophys. J.* **666**, 1189 (2007).
- [67] G. J. Fu, Y. Lei, H. Jiang, Y. M. Zhao, B. Sun, and A. Arima, *Phys. Rev. C* **84**, 034311 (2011).
- [68] B. Sun, P. W. Zhao and J. Meng, *Sci. China Ser. G - Phys. Mech. Astron.* **54**, 210 (2011).